Nonlinear Dyn (2013) 72:439–453
DOI 10.1007/s11071-012-0726-2

ORIGINAL PAPER

Nonlinear liquid sloshing in square tanks subjected to horizontal random excitation

Takashi Ikeda · Yuji Harata · Raouf A. Ibrahim

Received: 6 August 2012 / Accepted: 17 December 2012 / Published online: 8 January 2013

Abstract hing dynamics in a square tank are numerically investigated when the tank is subjected to horizontal, narrowband random ground excitation. The natural frequencies of the two predominant sloshing modes are identical and therefore 1:1 internal resonance may occur. Galerkin's method is applied to derive the modal equations of motion for nonlinear sloshing including higher modes. The Monte Carlo simulation is used to calculate response statistics such as mean square values and probability density functions (PDFs). The two predominant modes exhibit complex phenomena including "autoparametric interaction" because they are nonlinearly coupled with each other. The mean square responses of these two modes and the liquid elevation are found to differ significantly from those of the corresponding linear model, depending on the characteristics of the random ground excitation such as bandwidth, center frequency and excitation direction. It is found that the direction of the excitation is a significant factor in predicting the mean square responses. The frequency response curves for the same system subjected to equivalent harmonic excitation are also calculated and compared with the mean square responses to further explain the phenomena. Changing the liquid level causes the peak of the mean square response to shift. Furthermore, the risk of the liquid overspill from the tank is discussed by showing the three-dimensional distribution charts of the mean square responses of liquid elevations.

Keywords Sloshing · Autoparametric interaction · 1:1 internal resonance · Square liquid tank · Narrowband random excitation · Mean square value · Excitation direction · Probability density function

T. Ikeda (✉) · Y. Harata
Department of Mechanical Systems Engineering, Hiroshima University, 1-4-1 Kagamiyama, Higashi-Hiroshima, 739-8527, Japan
e-mail: tikeda@hiroshima-u.ac.jp

Y. Harata
e-mail: harata@hiroshima-u.ac.jp

R.A. Ibrahim
Department of Mechanical Engineering, Wayne State University, Detroit, MI 48202, USA
e-mail: aa1927@wayne.edu

Nomenclature

a_0	Amplitude of harmonic excitation with equivalent energy of random excitation ($=\sqrt{2\pi S_0/\gamma}$)
g	Acceleration of gravity
h	Liquid level
l	Tank length
P	Fluid pressure
p_{ij}	Natural frequency of sloshing mode (i, j)
S_0	Power spectrum density of white noise
t	Time
w	Tank width
(x, y, z)	Cartesian coordinate system (see Fig. 1)
x_g	Horizontal ground displacement
$W(t)$	Gaussian white noise

α	Excitation direction
γ	Bandwidth of a narrowband random excitation
η	Displacement of liquid surface
ρ	Fluid density
ϕ	Velocity potential function
ω	Angular frequency of equivalent harmonic excitation
Ω	Center frequency of narrowband random excitation
ζ_{ij}	Damping ratio of (i, j) sloshing mode

1 Introduction

Sloshing dynamics is one of the most important issues in mechanical, civil, marine and aeronautical engineering. The deterministic analyses of liquid sloshing dynamics are idealizations and simplifications of actual sloshing dynamics. The nature of excitation, however, may contain both periodic and random characteristics. Liquid storage tanks subjected to earthquakes, random sea waves acting on liquid cargo ships, and g-jitter in microgravity field are all examples of actual sloshing dynamics. A comprehensive review paper on nonlinear sloshing dynamics was compiled by Ibrahim et al. [1]. Housner [2] presented a linear sloshing model to investigate the responses of free surfaces in partially filled liquid tanks subjected to horizontal excitation, and his model has been widely used for seismic excitation in current design practice [3, 4]. However, it is well known that sloshing at large amplitudes exhibits nonlinear behavior, thus nonlinear models have been developed to obtain more accurate results. Groundbreaking studies on nonlinear sloshing behavior in cylindrical tanks subjected to horizontal, and/or vertical harmonic excitation were theoretically and experimentally examined by Hutton [5] and Abramson et al. [6]. Sloshing behavior in rectangular tanks under horizontal, harmonic excitation have also been investigated by Faltinsen [7] and Hayama et al. [8]. Three-dimensional sloshing in square tanks subjected to horizontal, harmonic excitation was theoretically investigated and their results were compared with experimental data by Faltinsen et al. [9, 10] and Ikeda et al. [11]. Because the two predominant sloshing modes in square tanks have an identical natural frequency and are nonlinearly coupled with each other, the internal resonance may occur. Therefore, sloshing may exhibit complex phenomena such as swirl motions and amplitude modulated motions (AMMs) including chaotic motions [11].

Nonlinear sloshing under random excitation has also been investigated. When the excitation is modeled as a random process, the free liquid surface response is described in terms of statistics such as mean square values, probability density functions (PDFs), autocorrelation functions, and power spectral density functions. Experimental measurements can be processed to estimate these statistics. Because of the nonlinear coupling of many sloshing modes, analytical stochastic approaches [12] would be extremely complicated and thus are not recommended. Instead, numerical simulations are usually applied and may be used to verify the validity of approximate analytical results if experimental results are not available. Dalzell [13] conducted experiments of horizontal, random sloshing in cylindrical tanks. He found that violent swirl motions of sloshing occurred for comparatively narrowband random excitation. Sakata et al. [14, 15], and Kimura et al. [16] theoretically investigated a cylindrical tank under horizontal, random base excitation using modal equations of motion for nonlinear sloshing. The excitation was modeled by a non-white random process with a dominant frequency. The heuristic approach was used to truncate the response statistical moment equations for three sloshing modes. Utsumi et al. [17, 18] used the same approach which was applied to rectangular and cylindrical tanks subjected to seismic excitation. They found that the nonlinearity of sloshing caused a non-zero-mean response to appear. Random responses of sloshing in a rectangular tank were also investigated using the finite-difference method by Chen et al. [19]. Nonlinear sloshing in a rectangular tank subjected to horizontal random excitation was investigated using the finite element method by Wang and Khou [20]. They obtained the time histories of waves and hydrodynamic forces, PDFs and power spectra and found that narrowband excitation caused larger wave responses to appear. Sriram et al. [21] also used the finite element method to investigate nonlinear sloshing in rectangular tanks subjected to horizontal and vertical random excitation. They observed high amplitudes of the first sloshing mode due to the primary and parametric resonances. Nasar et al. [22] experimentally investigated sloshing in a rectangular tank mounted on a barge subjected to random wave excitation. They studied the influences of liquid levels and excitation frequencies on odd and even

sloshing modes. Furthermore, nonlinear responses of elastic structures with cylindrical tanks subjected to vertical random excitation were also investigated [23–25]. However, random responses of nonlinear sloshing in square tanks have not yet been investigated in detail.

The present paper extends the work of Ikeda et al. [26] by investigating nonlinear sloshing behavior in square tanks subjected to horizontal, random ground excitation using the same model as that in reference [11]. The natural frequencies of the two predominant sloshing modes are identical and therefore 1:1 internal resonance may occur. Galerkin's method is employed to derive the nonlinear modal equations of motion for sloshing. These modal equations are solved using the Monte Carlo simulation, and the mean square responses of the two predominant sloshing modes are calculated. These responses are compared with the theoretical results for the corresponding linear model. PDFs of liquid elevation are also calculated. The influences of the center frequency, bandwidth and excitation direction of the random excitation, and the liquid level on the mean square responses are examined. The frequency response curves for the same system subjected to harmonic excitation are calculated when the energy of the harmonic excitation is equivalent to that of the random excitation. These curves are then compared with the mean square responses in the case of random excitation to further explain the nonlinear behavior depending on the excitation direction. Finally, three-dimensional distribution charts of liquid elevations are used to discuss the risk of the liquid overspill.

2 Theoretical analysis

2.1 Equations of motion

Figure 1 shows a theoretical model for sloshing in a square tank with length l, breadth w, and liquid filled to level h. The Cartesian coordinate system O–xyz is fixed to the tank where the xy-plane coincides with the undisturbed free surface of the liquid. The tank is subjected to horizontal, random ground excitation $x_g(t)$, and the excitation direction deviates from the tank length by angle α. In the theoretical analysis, the liquid is assumed to be perfect; hence the velocity potential $\phi(x, y, z, t)$ can be introduced. $P(x, y, z, t)$ is the fluid pressure, ρ is the fluid density, and $\eta(x, y, t)$ is the liquid elevation at position (x, y) in the tank. The following dimensionless quantities are introduced:

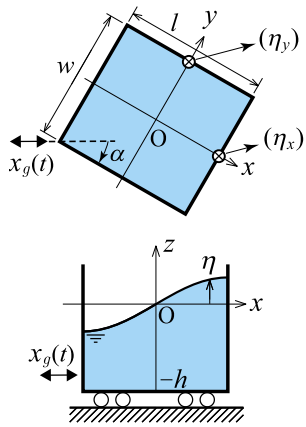

Fig. 1 The model for theoretical analysis

$$
\begin{aligned}
&h' = h/l, w' = w/l, \qquad x' = x/l, \qquad x'_g = x_g/l,\\
&y' = y/l, \qquad P' = P/\left(\rho l^2 p_{10}^2\right), \qquad z' = z/l,\\
&\eta' = \eta/l, \qquad \phi' = \phi/\left(l^2 p_{10}\right), \qquad \lambda'_{ij} = \lambda_{ij} l,\\
&p'_{ij} = p_{ij}/p_{10}, \qquad t' = p_{10} t,
\end{aligned}
\tag{1}
$$

where

$$
\begin{aligned}
&\lambda_{ij} = \pi\sqrt{(i/l)^2 + (j/w)^2},\\
&p_{ij} = \sqrt{g\lambda_{ij}\tanh(\lambda_{ij} h)}.
\end{aligned}
\tag{2}
$$

Here, g is the acceleration of gravity, and p_{ij} represents the natural frequency of (i, j) sloshing mode. Figures 2(a), 2(b) and 2(c) show the shapes of (1, 0), (0, 1), and (1, 1) sloshing modes, respectively. The nodal lines of (1, 0) and (0, 1) modes coincide with the y- and x-axes, respectively. The nodal lines of (1, 1) mode coincide with the x- and y-axes. All primes " ′" in (1) will hereafter be omitted for simplicity, although the quantities are dimensionless in the theoretical analysis and results.

Laplace's equation and Euler's energy equation for the fluid motion are expressed in dimensionless form, respectively, as

$$
\frac{\partial^2\phi}{\partial x^2} + \frac{\partial^2\phi}{\partial y^2} + \frac{\partial^2\phi}{\partial z^2} = 0, \tag{3}
$$

$$
\begin{aligned}
&\frac{\partial\phi}{\partial t} + \frac{1}{2}\left[\left(\frac{\partial\phi}{\partial x}\right)^2 + \left(\frac{\partial\phi}{\partial y}\right)^2 + \left(\frac{\partial\phi}{\partial z}\right)^2\right] + \frac{z}{\psi_{10}} + P\\
&\quad = -\ddot{x}_g x\cos\alpha - \ddot{x}_g y\sin\alpha,
\end{aligned}
\tag{4}
$$

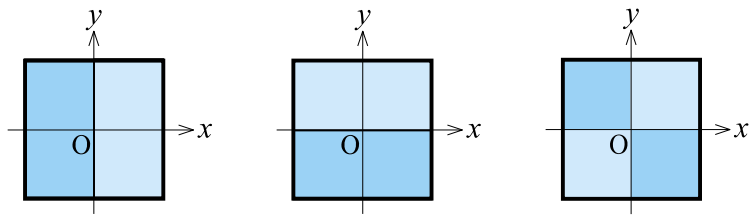

(a) (1, 0) mode (b) (0, 1) mode (c) (1, 1) mode

Fig. 2 Mode shapes of sloshing

where $\psi_{10} = \lambda_{10}\tanh(\lambda_{10}h)$. The boundary conditions for the fluid velocity at the tank walls and bottom are

$$\begin{aligned} &\frac{\partial\phi}{\partial x} = 0 \quad (\text{at } x = \pm 1/2), \\ &\frac{\partial\phi}{\partial y} = 0 \quad (\text{at } y = \pm w/2), \\ &\frac{\partial\phi}{\partial z} = 0 \quad (\text{at } z = -h). \end{aligned} \tag{5}$$

In addition, the kinematic boundary condition at the liquid free surface is

$$\frac{\partial\phi}{\partial z} = \frac{\partial\eta}{\partial t} + \frac{\partial\phi}{\partial x}\frac{\partial\eta}{\partial x} + \frac{\partial\phi}{\partial y}\frac{\partial\eta}{\partial y} \quad (\text{at } z = \eta). \tag{6}$$

Because $P = 0$ at the free liquid surface, the boundary condition for (4) is

$$\begin{aligned} &\frac{\partial\phi}{\partial t} + \frac{1}{2}\left[\left(\frac{\partial\phi}{\partial x}\right)^2 + \left(\frac{\partial\phi}{\partial y}\right)^2 + \left(\frac{\partial\phi}{\partial z}\right)^2\right] + \frac{\eta}{\psi_{10}} \\ &\quad = -\ddot{x}_g x\cos\alpha - \ddot{x}_g y\sin\alpha \quad (\text{at } z = \eta). \end{aligned} \tag{7}$$

The ground excitation $x_g(t)$ is assumed to be generated from the second-order, linear shaping filter as follows:

$$\ddot{x}_g + \gamma\dot{x}_g + \Omega^2 x_g = \Omega W(t), \tag{8}$$

where $W(t)$ is a zero-mean stationary Gaussian white noise process with variance σ_W^2 and constant power spectral density intensity S_0. Here, γ is the bandwidth and Ω is the center frequency of $x_g(t)$. Note that the mean square value of $x_g(t)$ is well documented in many references (see, e.g., [27]) and is given by the expression $E[x_g^2] = 2\pi S_0/\gamma$. Equations (3) through (8) constitute the boundary value problem of sloshing dynamics in square tanks.

2.2 Modal equations of motion for sloshing

Galerkin's method is used to derive modal equations of motion for sloshing. Here, ϕ and η are assumed in terms of the eigenfunctions which can be obtained from the corresponding linear system, as follows:

$$\begin{aligned} \phi(x,y,z,t) = &\sum_{i=0}^{\infty}\sum_{j=0}^{\infty} a_{ij}(t)U_{ij}(x,y) \\ &\times \cosh\{\lambda_{ij}(z+h)\}/\cosh(\lambda_{ij}h), \end{aligned} \tag{9a}$$

$$\eta(x,y,t) = \sum_{i=0}^{\infty}\sum_{j=0}^{\infty} b_{ij}(t)U_{ij}(x,y), \tag{9b}$$

in which $U_{ij}(x,y)$ represent eigenfunctions as follows:

$$U_{ij}(x,y) = \begin{cases} \sin(\lambda_{i0}x)\sin(\lambda_{0j}y) & (i = 2m+1,\ j = 2n+1) \\ \sin(\lambda_{i0}x)\cos(\lambda_{0j}y) & (i = 2m+1,\ j = 2n) \\ \cos(\lambda_{i0}x)\sin(\lambda_{0j}y) & (i = 2m,\ j = 2n+1) \\ \cos(\lambda_{i0}x)\cos(\lambda_{0j}y) & (i = 2m,\ j = 2n), \end{cases} \tag{10}$$

where m and n are integers. Note that λ_{ij} in (10) represent dimensionless quantities given by (1) and (2). Here, $a_{ij}(t)$ and $b_{ij}(t)$ in (9a), (9b) are unknown functions of time. The coordinates x and y in (4) and (7) are expanded in terms of the eigenfunctions of (10) as

$$x = \sum_{i=1}^{\infty}[r_{i0}U_{i0}(x,y)], \qquad y = \sum_{j=1}^{\infty}[r_{0j}U_{0j}(x,y)], \tag{11}$$

where the coefficients r_{i0} and r_{0j} are determined by the method adopted in reference [11] as follows:

$$\begin{aligned} r_{i0} &= \begin{cases} (-1)^{\frac{i-1}{2}}\frac{4}{i^2\pi^2} & (i = 1,3,5,\ldots) \\ 0 & (i = 0,2,4,\ldots), \end{cases} \\ r_{0j} &= \begin{cases} (-1)^{\frac{j-1}{2}}\frac{4w}{i^2\pi^2} & (j = 1,3,5,\ldots) \\ 0 & (j = 0,2,4,\ldots). \end{cases} \end{aligned} \tag{12}$$

Here, ε is introduced as a bookkeeping parameter to determine the approximate solutions when the two sloshing modes (1, 0) and (0, 1) predominantly appear.

Therefore, the orders of $a_{ij}(t)$, $b_{ij}(t)$, x_g, and the system parameters are assumed as follows:

$$\begin{aligned}
&a_{10}, a_{01}, b_{10}, b_{01}, \zeta_{ij} \approx O\left(\varepsilon^{1/3}\right),\\
&a_{20}, a_{02}, a_{30}, a_{03}, a_{11}, b_{20}, b_{02}, b_{30}, b_{03}, b_{11}\\
&\quad \approx O\left(\varepsilon^{2/3}\right),\\
&a_{i0}, a_{0j}, a_{ij}, b_{i0}, b_{0j}, b_{ij}, x_g \approx O\left(\varepsilon^{3/3}\right)\\
&\quad (i \geq 4,\ j \geq 4).
\end{aligned} \tag{13}$$

Equation (13) follows Hutton's ordering [5] for cylindrical tanks, that is, (1, 0) and (0, 1) modes are of $O(\varepsilon^{1/3})$, (2, 0), (1, 1), and (0, 2) modes are of $O(\varepsilon^{2/3})$, and (3, 0), (1, 2), (2, 1), and (0, 3) modes are of $O(\varepsilon^{2/3})$. However, (1, 2) and (2, 1) modes are not considered because they are not nonlinearly coupled with the two predominant modes [11]. Furthermore, the damping ratios ζ_{ij} are assumed to be of $O(\varepsilon^{1/3})$ in order to consider the damping effects for all modes in the modal equations. The validity of this ordering was confirmed because the theoretical results agreed well with the experimental data in the case of harmonic excitation [11].

Equations (6) and (7) are expanded near $\eta = 0$, and (9a), (9b) are substituted into these two resulting equations. By equating the coefficients of $\sin(\lambda_{10}x)$, $\sin(\lambda_{01}y)$, $\cos(\lambda_{20}x)$, $\cos(\lambda_{02}y)$, $\sin(\lambda_{30}x)$, $\sin(\lambda_{03}y)$ and $\sin(\lambda_{10}x)\sin(\lambda_{01}y)$ on both sides of these two equations within the accuracy of $O(\varepsilon)$, and eliminating a_{ij} from the resulting equations, one can obtain the modal equations of motion for sloshing as follows:

$$\begin{aligned}
&\ddot{b}_{10} + 2\zeta_{10}\dot{b}_{10} + b_{10} + H_1(b_{10}, b_{01}, b_{20}, b_{11})\\
&\quad = -\psi_{10} r_{10} \ddot{x}_g \cos\alpha\\
&\ddot{b}_{01} + 2\zeta_{01}\omega_{01}\dot{b}_{01} + \omega_{01}^2 b_{01} + H_2(b_{10}, b_{01}, b_{02}, b_{11})\\
&\quad = -\psi_{01} r_{01} \ddot{x}_g \sin\alpha\\
&\ddot{b}_{20} + 2\zeta_{20}\omega_{20}\dot{b}_{20} + \omega_{20}^2 b_{20} + H_3(b_{10}, b_{30}) = 0\\
&\ddot{b}_{02} + 2\zeta_{02}\omega_{02}\dot{b}_{02} + \omega_{02}^2 b_{02} + H_4(b_{01}, b_{03}) = 0\\
&\ddot{b}_{30} + 2\zeta_{30}\omega_{30}\dot{b}_{30} + \omega_{30}^2 b_{30} + H_5(b_{10}, b_{20})\\
&\quad = -\psi_{30} r_{30} \ddot{x}_g \cos\alpha\\
&\ddot{b}_{03} + 2\zeta_{03}\omega_{03}\dot{b}_{03} + \omega_{03}^2 b_{03} + H_6(b_{01}, b_{02})\\
&\quad = -\psi_{03} r_{03} \ddot{x}_g \sin\alpha\\
&\ddot{b}_{11} + 2\zeta_{11}\omega_{11}\dot{b}_{11} + \omega_{11}^2 b_{11} + H_7(b_{10}, b_{01}) = 0,
\end{aligned} \tag{14}$$

where $\omega_{ij}^2 = \psi_{ij}/\psi_{10}$ and $\psi_{ij} = \lambda_{ij}\tanh(\lambda_{ij}h)$. Note that linear viscous damping terms $2\zeta_{ij}\omega_{ij}\dot{b}_{ij}$ are incorporated in (14) to consider the damping effect of sloshing. The nonlinear terms H_m $(m = 1, 2, \ldots, 7)$ in (14) are

$$\begin{aligned}
H_1 &= S_1\dot{b}_{10}\dot{b}_{20} + S_2\dot{b}_{01}\dot{b}_{11} + S_3\dot{b}_{10}^2 b_{10} + S_4\dot{b}_{01}^2 b_{10}\\
&\quad + S_5\dot{b}_{10}\dot{b}_{01} b_{01}\\
&\quad + S_6 b_{10} b_{20} + S_7 b_{01} b_{11} + S_8 b_{10}^3 + S_9 b_{01}^2 b_{10}\\
H_2 &= S_{10}\dot{b}_{01}\dot{b}_{02} + S_{11}\dot{b}_{10}\dot{b}_{11} + S_{12}\dot{b}_{01}^2 b_{01}\\
&\quad + S_{13}\dot{b}_{10}^2 b_{01} + S_{14}\dot{b}_{10}\dot{b}_{01} b_{10} + S_{15} b_{01} b_{02}\\
&\quad + S_{16} b_{10} b_{11} + S_{17} b_{01}^3 + S_{18} b_{10}^2 b_{01}\\
H_3 &= S_{19}\dot{b}_{10}^2 + S_{20}\dot{b}_{10}\dot{b}_{30} + S_{21} b_{10}^2 + S_{22} b_{10} b_{30}\\
H_4 &= S_{23}\dot{b}_{01}^2 + S_{24}\dot{b}_{01}\dot{b}_{03} + S_{25} b_{01}^2 + S_{26} b_{01} b_{03}\\
H_5 &= S_{27}\dot{b}_{10}\dot{b}_{20} + S_{28}\dot{b}_{10}^2 b_{10} + S_{29} b_{10} b_{20} + S_{30} b_{10}^3\\
H_6 &= S_{31}\dot{b}_{01}\dot{b}_{02} + S_{32}\dot{b}_{01}^2 b_{01} + S_{33} b_{01} b_{02} + S_{34} b_{01}^3\\
H_7 &= S_{35}\dot{b}_{10}\dot{b}_{01} + S_{36} b_{10} b_{01},
\end{aligned} \tag{15}$$

where the symbols S_n $(n = 1, 2, \ldots, 36)$ are constants defined by the dimensions of the tank, h and w, and their complete expressions are omitted here. Because the nonlinear terms of b_{10} and b_{01} are included in H_1 and H_2 of (15), (1, 0), and (0, 1) modes are nonlinearly coupled and form an autoparametric system. Higher mode (2, 0) is nonlinearly coupled with both (1, 0) and (3, 0) modes. Note that b_{10} is included in H_5 for (3, 0) mode, but b_{30} is not included in H_1 for (1, 0) mode. Hence, (1, 0) mode influences (3, 0) mode, but the opposite is not true. The same holds for (0, 1), (0, 2), and (0, 3) modes. Furthermore (1, 1) mode is nonlinearly coupled with the two predominant modes because it is also included in H_1 and H_2 of (15). This mode plays a significant role for three-dimensional liquid sloshing in square tanks.

2.3 Nonlinear uncoupled system

Figures 3(a) and 3(b) show the schematic diagrams for energy flow represented by the arrows in the nonlinear coupled and uncoupled systems, respectively. The four components of the ground excitation transfer energy directly to (1, 0), (0, 1), (3, 0), and (0, 3) modes depending on the value of α. Figure 3(a) corresponds to the autoparametric system (14) which exhibits three-dimensional sloshing. In order to examine the influence of nonlinear coupling between the two predominant modes in square tanks, the hypothetical, nonlinear uncoupled system is considered in Fig. 3(b). In this hypothetical system, (1, 0) and (0, 1) modes are not nonlinearly coupled, i.e., b_{01} in H_1, and b_{10} in H_2 of (15)

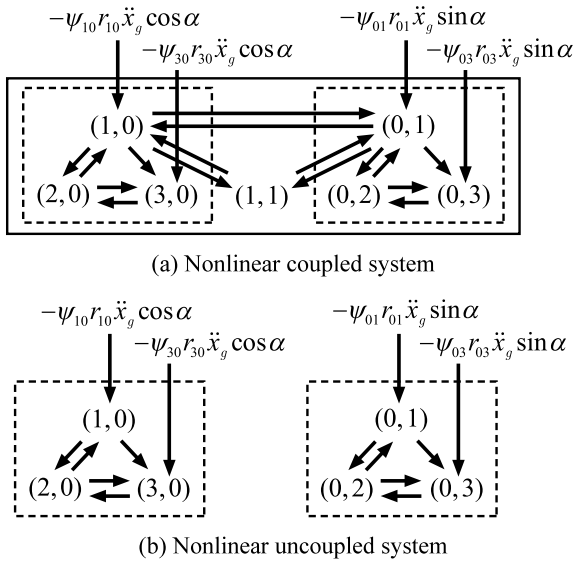

Fig. 3 Schematic diagrams for energy flow

are assumed to be zero, and (1, 1) is not considered. This nonlinear uncoupled system consists of two independent systems which are governed by (1, 0), (2, 0), and (3, 0) modes, and (0, 1), (0, 2), and (0, 3) modes, as shown in Fig. 3(b). The sloshing in these systems is two-dimensional and behaves as if two rectangular tanks are subjected to random ground excitation. The mean square responses of the nonlinear uncoupled system are calculated to compare with those of the nonlinear coupled system.

2.4 Theoretical random responses in the corresponding linear model

The linearized equations of motion for (1, 0) and (0, 1) sloshing modes are obtained from (14) as

$$\begin{aligned}\ddot{b}_{10}+2\zeta_{10}\dot{b}_{10}+b_{10}&=-\psi_{10}r_{10}\ddot{x}_g\cos\alpha\\ \ddot{b}_{01}+2\zeta_{01}\omega_{01}\dot{b}_{01}+\omega_{01}^2 b_{01}&=-\psi_{01}r_{01}\ddot{x}_g\sin\alpha.\end{aligned}\tag{16}$$

The autocorrelation functions $R_{b_{10}}(\tau)$ and $R_{b_{01}}(\tau)$ of $b_{10}(t)$ and $b_{01}(t)$ can be, respectively, expressed by

$$\begin{aligned}R_{b_{10}}(\tau)&=\int_{-\infty}^{\infty}\left|G_1(j\omega)\right|^2 S_W(\omega)e^{j\omega\tau}\,\mathrm{d}\omega\\ R_{b_{01}}(\tau)&=\int_{-\infty}^{\infty}\left|G_2(j\omega)\right|^2 S_W(\omega)e^{j\omega\tau}\,\mathrm{d}\omega,\end{aligned}\tag{17}$$

where $S_W(\omega)=S_0$ is the power spectral density of the white noise $W(t)$. Here, $G_1(j\omega)$ and $G_2(j\omega)$ represent the complex frequency response functions, which can be obtained from the transfer functions, defined as the ratios of the responses $b_{10}(t)$ and $b_{01}(t)$ to the input $W(t)$, respectively, as follows:

$$\begin{aligned}G_1(s)&=\frac{\Omega}{s^2+\gamma s+\Omega^2}\cdot\frac{-\psi_{10}r_{10}\cos\alpha\cdot s^2}{s^2+2\zeta_{10}s+1}\\ G_2(s)&=\frac{\Omega}{s^2+\gamma s+\Omega^2}\cdot\frac{-\psi_{01}r_{01}\sin\alpha\cdot s^2}{s^2+2\zeta_{01}\omega_{01}s+\omega_{01}^2}.\end{aligned}\tag{18}$$

Substituting $\tau=0$ into (17) gives the mean square responses

$$\begin{aligned}E\left[b_{10}^2\right]&=R_{b_{10}}(0)=S_0\int_{-\infty}^{\infty}\left|G_1(j\omega)\right|^2\mathrm{d}\omega\\ &=S_0\cdot I_1/I_2\end{aligned}\tag{19a}$$

$$\begin{aligned}E\left[b_{01}^2\right]&=R_{b_{01}}(0)=S_0\int_{-\infty}^{\infty}\left|G_2(j\omega)\right|^2\mathrm{d}\omega\\ &=S_0\cdot I_3/I_4,\end{aligned}\tag{19b}$$

where

$$\begin{aligned}I_1&=\pi S_0\Omega^2\left(\gamma+2\zeta_{10}\Omega^2\right)(\psi_{10}r_{10}\cos\alpha)^2,\\ I_2&=(2\zeta_{10}+\gamma)\left(\Omega^2+2\zeta_{10}\gamma+1\right)\left(\gamma+2\zeta_{10}\Omega^2\right)\\ &\quad-\Omega^2(2\zeta_{10}+\gamma)^2-\left(\gamma+2\zeta_{10}\Omega^2\right)^2\\ I_3&=\pi S_0\Omega^2\left(\gamma\omega_{01}^2+2\zeta_{01}\Omega^2\right)(\psi_{01}r_{01}\sin\alpha)^2,\\ I_4&=(2\zeta_{01}\omega_{01}+\gamma)\left(\Omega^2+2\zeta_{01}\omega_{01}\gamma+\omega_{01}^2\right)\\ &\quad\times\left(\gamma\omega_{01}^2+2\zeta_{01}\Omega^2\right)-\Omega^2\omega_{01}^2(2\zeta_{01}+\gamma)^2\\ &\quad-\left(\gamma\omega_{01}^2+2\zeta_{01}\Omega^2\right)^2.\end{aligned}\tag{20}$$

Equation (19a), (19b) is given in closed form and used to calculate the theoretical curves of the mean square values for the linear system which will be compared with the simulation results for the nonlinear coupled system.

3 Numerical results

Figure 4 shows the time histories for white noise $W(t)$, ground motion $x_g(t)$, sloshing modal amplitudes b_{10}, b_{01}, and b_{11}, and liquid elevations η_x and η_y. These liquid elevations are measured at positions $(x, y) = (0.5, 0)$ and $(0, w/2)$ over the x- and y-axes, respectively, as shown in Fig. 1. These time histories are calculated by the Monte Carlo simulation of (8) and (14) for the nonlinear coupled system. The values of the system parameters are $h = 0.6$, $w = 1.0$, $\zeta_{ij} = 0.013$, $\alpha = 0°$, $\gamma = 0.03$, $S_0 = 1.0 \times 10^{-7}$ and $\Omega =$

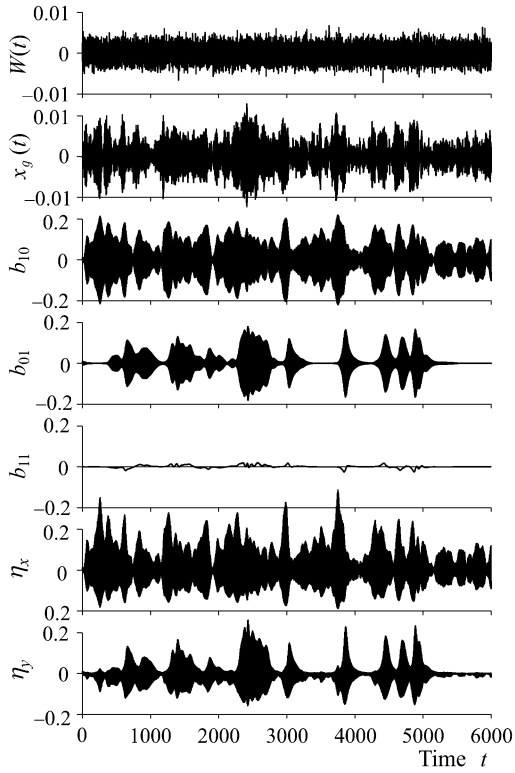

Fig. 4 Time histories when $h = 0.6, w = 1.0, \zeta_{ij} = 0.013$, $\alpha = 0°, \gamma = 0.03, S_0 = 1.0 \times 10^{-7}$ and $\Omega = 0.98$

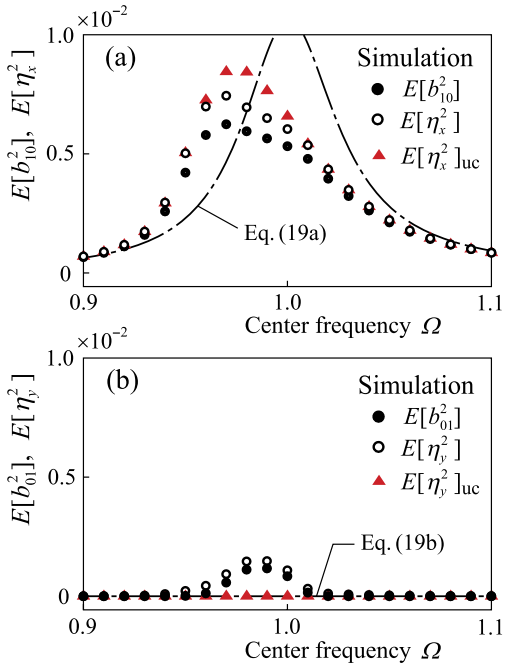

Fig. 5 Mean square responses showing the influence of the center frequency Ω when $\gamma = 0.03$ and the other values of the parameters are the same as those in Fig. 4. (**a**) $E[b_{10}^2]$, $E[\eta_x^2]$ and $E[\eta_x^2]_{\mathrm{uc}}$ for (1, 0) mode; (**b**) $E[b_{01}^2]$, $E[\eta_y^2]$ and $E[\eta_y^2]_{\mathrm{uc}}$ for (0, 1) mode

0.98. The Runge–Kutta–Gill method is used to conduct the numerical simulation. The time step of the simulation is set as $\Delta t = 0.25$, hence the Nyquist frequency $\omega_N = 2\pi/(2\Delta t) = \pi/\Delta t = 12.57$. The Gaussian white noise $W(t)$ is generated from a random number series with a zero-mean value and variance $\sigma_W^2 = 2\pi S_0/\Delta t$ by using a FORTRAN subroutine based on the Box–Muller method [28]. Because (1, 0) mode is directly excited by the random ground excitation when $\alpha = 0°$, b_{10} and η_x oscillate violently. Furthermore, b_{01} and η_y oscillate intermittently because (0, 1) mode is nonlinearly coupled with (1, 0) mode. This is known as "autoparametric interaction." It can also be seen that (1, 1) mode appears and its constant component fluctuates because it is autoparametrically excited by (1, 0) mode when $\alpha = 0°$.

3.1 Influence of bandwidth

The time history records are processed to estimate the mean square responses of the sloshing modal amplitudes and the liquid elevations. The simulation results of the mean square responses are shown in Fig. 5, and the values of the parameters are the same as those in Fig. 4. Figure 5(a) shows (1, 0) mode and liquid elevation η_x, and Fig. 5(b) shows (0, 1) mode and η_y. The mean square values $E[b_{10}^2]$ and $E[b_{01}^2]$ are plotted by "●", and $E[\eta_x^2]$ and $E[\eta_y^2]$ are plotted by "○". Furthermore, "▲" represents the mean square values $E[\eta_x^2]_{\mathrm{uc}}$ and $E[\eta_y^2]_{\mathrm{uc}}$ which are obtained from the hypothetical, nonlinear uncoupled system defined in Sect. 2.3. All mean square values are estimated from the time histories over the time duration $t = 1000$–6000 in order to avoid the influence of the transient duration and to satisfy the convergence of these values using 100 different sets of random number series. The dash-dotted line represents the theoretical curves calculated from (19a), (19b) for the corresponding linear model. Because "○" includes the components of higher sloshing modes, it appears at slightly larger values than "●". The simulation results are close to the theoretical curve (19a) near $\Omega = 0.9$ and 1.1 in Fig. 5(a) when sloshing appears at low amplitudes. However, in Figs. 5(a) and 5(b), the simu-

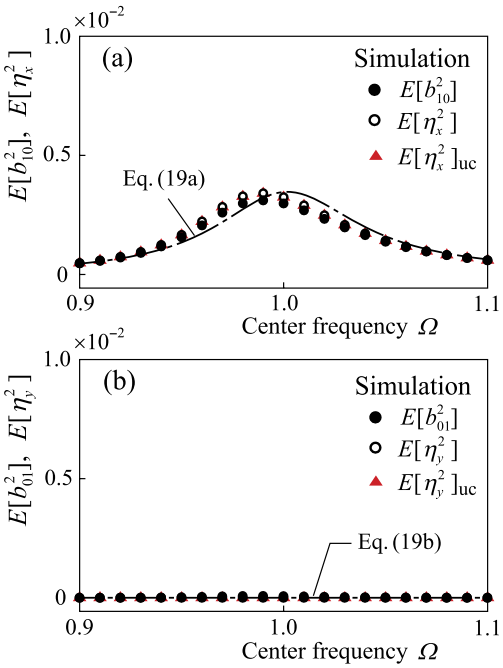

Fig. 6 Same as Fig. 5, but $\gamma = 0.06$. (**a**) $E[b_{10}^2]$ and $E[\eta_x^2]$ for (1, 0) mode; (**b**) $E[b_{01}^2]$ and $E[\eta_y^2]$ for (0, 1) mode

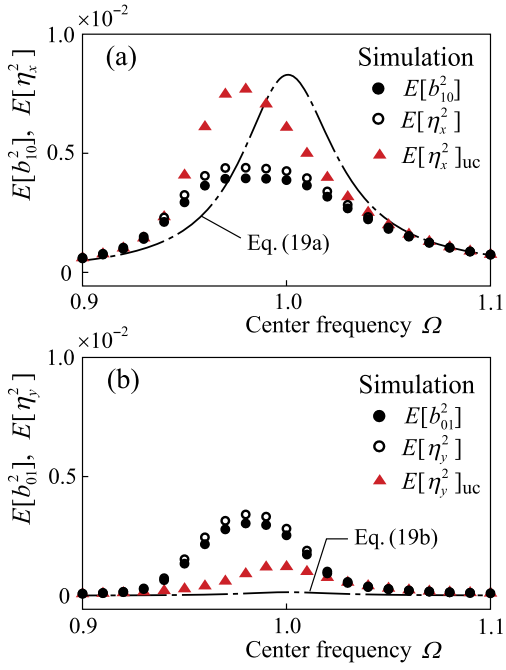

Fig. 7 Same as Fig. 5, but $\alpha = 20°$. (**a**) $E[b_{10}^2]$, $E[\eta_x^2]$ and $E[\eta_x^2]_{\mathrm{uc}}$ for (1, 0) mode; (**b**) $E[b_{01}^2]$, $E[\eta_y^2]$ and $E[\eta_y^2]_{\mathrm{uc}}$ for (0, 1) mode

lation results "●" and "○" deviate significantly from the theoretical curves near $\Omega = 1.0$. Although (0, 1) mode is not directly excited by random ground excitation, $E[b_{01}^2]$ and $E[\eta_y^2]$ appear at small values near $\Omega = 1.0$. This is because (0, 1) mode is autoparametrically excited by (1, 0) mode. "▲" in Fig. 5(a) is larger than "○", and "▲" in Fig. 5(b) is not excited because the autoparametric interaction does not occur in the nonlinear uncoupled system. The difference between "○" and "▲" may correspond to the amount of the energy transferred from (1, 0) mode to (0, 1) mode though the nonlinear coupling terms. The values $E[b_{10}^2]$ on the left hand side of $\Omega = 1.0$ are large and correspond to a soft-type Duffing oscillator under harmonic excitation because the liquid level $h = 0.6$ is comparatively high.

Figure 6 shows the influence of the bandwidth of random excitation on the mean square responses when only the value of the bandwidth is changed from $\gamma = 0.03$ in Fig. 5 to 0.06. As γ increases, the mean square values $E[b_{10}^2]$ flatten and the simulation results approach the theoretical curve (19a). In addition, the mean square values $E[b_{01}^2]$ are close to zero. This implies that the autoparametric interaction between (1, 0) and (0, 1) modes is not significant. Note that each "▲" in Fig. 6 appears at almost the same value as each "○" for the same reason. Further increasing the bandwidth would probably result in a flat line even for (1, 0) mode.

3.2 Influence of excitation direction

The influence of excitation direction on the mean square responses of nonlinear sloshing in a square tank is the primary focus of the present study and is examined by changing the value of α. Figures 7, 8, and 10 show the dependence of the mean square responses on the center excitation frequency Ω, when only the value of α is changed, from $\alpha = 0°$ in Fig. 5 to 20°, 40° and 45°, respectively. When $\alpha \neq 0°$, (1, 0) and (0, 1) sloshing modes are both directly excited by random ground excitation. In Fig. 7(a) when $\alpha = 20°$, the peak of "●" for $E[b_{10}^2]$ becomes lower than that in Fig. 5(a) but still deviates from the theoretical curve (19a). On the contrary, the peak of $E[b_{01}^2]$ in Fig. 7(b) becomes higher than that in Fig. 5(b). Furthermore, the peak of the theoretical curve (19b) is extremely low although (0, 1) mode is also directly excited in the linear system. The difference between "▲" and "○" near $\Omega = 1.0$ in Fig. 7 is larger than that in Fig. 5. This is because "▲"

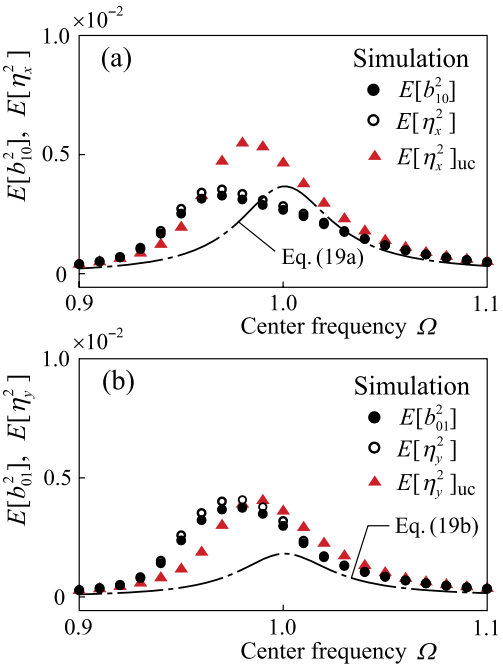

Fig. 8 Same as Fig. 5, but $\alpha = 40°$. (**a**) $E[b_{10}^2]$, $E[\eta_x^2]$ and $E[\eta_x^2]_{\rm uc}$ for (1, 0) mode; (**b**) $E[b_{01}^2]$, $E[\eta_y^2]$ and $E[\eta_y^2]_{\rm uc}$ for (0, 1) mode

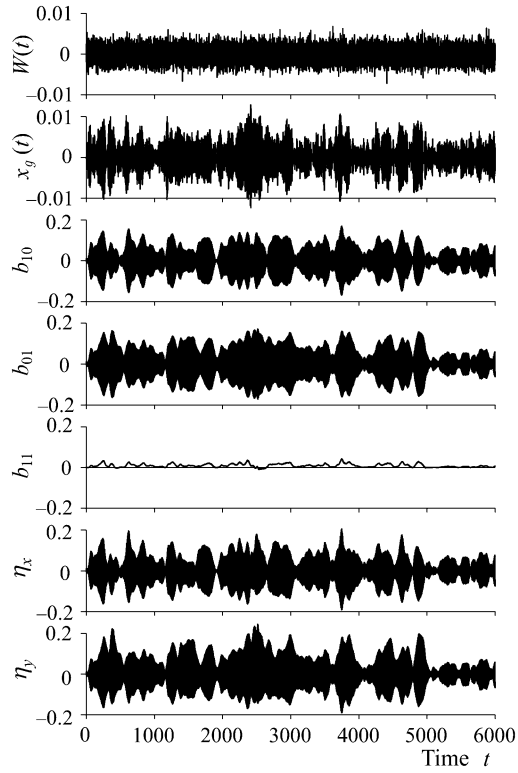

Fig. 9 Time histories at $\Omega = 0.98$ in Fig. 8

in Fig. 7(a) receives more energy from the ground excitation, whereas "○" transfers some of this energy to (0, 1) mode due to the autoparametric interaction. This is also why both "○" and "●" in Fig. 7(b) for (0, 1) mode appear at higher values than "▲" even though (0, 1) mode receives less energy from the ground excitation.

When $\alpha = 40°$, both the theoretical curve (19a) and "▲" in Fig. 8(a) still appear at larger values than (19a) and "▲" in Fig. 8(b), respectively. Interestingly, this is not true for the coupled system. Note that "○" appears at smaller values in Fig. 8(a) than 8(b) near the peak at $\Omega = 0.98$. As the value of α approaches 45°, (1, 0) mode receives increasingly less energy from the ground excitation, while (0, 1) mode receives increasingly more. Furthermore, the autoparametric interaction continues to occur, thus some of this energy is exchanged between the two predominant modes, (1, 0) and (0, 1), and the higher mode (1, 1). It can then be assumed that when $\alpha = 40°$, the total energy of (1, 0) mode is less than that of (0, 1) mode due to the autoparametric interaction. When the amplitude of sloshing is high, the influence of the autoparametric interaction is greater resulting in the peak of Fig. 8(b) being higher than that of Fig. 8(a). Figure 9 shows the time histories at $\Omega = 0.98$ in Fig. 8. Note that the time histories of $W(t)$ and $x_g(t)$ in Fig. 9 are the same as those in Fig. 4 because identical random number series and initial conditions are used. However, it can be seen that b_{01} and η_y oscillate more frequently at higher amplitudes than b_{10} and η_x. This confirms that $E[\eta_y^2]$ is larger than $E[\eta_x^2]$ near $\Omega = 0.98$ in Fig. 8.

For $\alpha = 45°$ in Fig. 10, the simulation results and the theoretical curves are identical in Figs. 10(a) and 10(b) because (1, 0) and (0, 1) modes receive the same amount of energy from the random ground excitation. However, the coupled and uncoupled systems behave like a soft-spring Duffing system when the liquid level is comparatively high. Thus, the peaks of "○" and "▲" appear at higher values than those of the theoretical curves (19a), (19b) and shift to the left of the center frequency $\Omega = 1.0$. Furthermore, (1, 1) mode is autoparametrically excited by and absorbs energy from (1, 0) and (0, 1) modes, and it may cause the peaks of "○" and "●" to appear further to the left, and at lower mean square values than those of "▲".

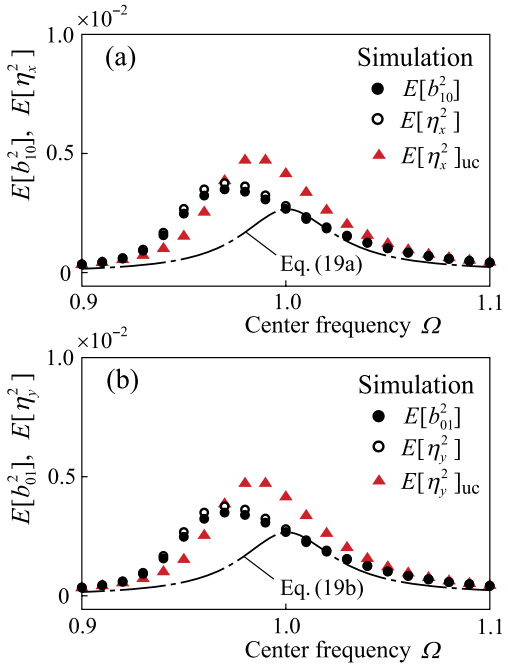

Fig. 10 Same as Fig. 5, but $\alpha = 45°$. (**a**) $E[b_{10}^2]$, $E[\eta_x^2]$ and $E[\eta_x^2]_{\rm uc}$ for (1, 0) mode; (**b**) $E[b_{01}^2]$, $E[\eta_y^2]$ and $E[\eta_y^2]_{\rm uc}$ for (0, 1) mode

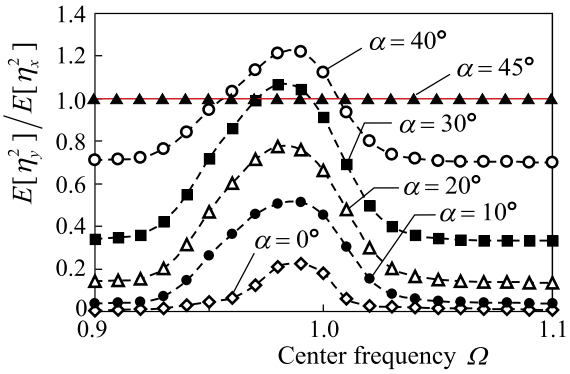

Fig. 11 The ratio of $E[\eta_y^2]$ to $E[\eta_x^2]$ depending on the excitation direction, including Figs. 5, 7, 8, and 10

Figure 11 shows the dependence of the ratio $E[\eta_y^2]$ to $E[\eta_x^2]$ on Ω in terms of the excitation direction, including Figs. 5, 7, 8 and 10 for $\alpha = 0°, 20°, 40°$ and 45°. The purpose of this figure is to reveal the degree of interaction between the two predominant modes. When $\alpha = 45°$ and the means square responses of (1, 0) and (0, 1) modes are identical, the ratio $E[\eta_y^2]/E[\eta_x^2]$ equals 1.0 for any value of Ω. This ratio is less than 1.0 when α is less than 20°, thus (1, 0) mode always appears at higher values than (0, 1) mode. As α increases, the ratio gradually approaches 1.0 near $\Omega = 1.0$. Because the ratio is less than 1.0 when α is less than 20° but exceeds 1.0 for $0.97 < \Omega < 1.0$ when $\alpha = 30°$, a critical value α_c exists in the range $20° < \alpha < 30°$, where the peak of the ratio $E[\eta_y^2]/E[\eta_x^2]$ equals 1.0. When $\alpha < \alpha_c$, it can be assumed that this ratio would be less than 1.0 and thus the total energy of (1, 0) mode is greater than that of (0, 1) mode. When $\alpha > \alpha_c$, however, this ratio would be greater than 1.0 and the total energy of (1, 0) mode would be less than (0, 1) mode depending on the value of Ω. Thus when $\alpha = 40°$, although $E[\eta_x^2]$ is expected to be larger than $E[\eta_y^2]$ because the component of the ground excitation in the x-direction of the tank is larger than that in the y-direction, the opposite results occur for $0.955 < \Omega < 1.017$. When the bandwidth is narrow, this result is similar to that of a system under harmonic excitation where multivalued response curves are observed [11]. Therefore, in order to clarify this result, the frequency response curves for the system subjected to harmonic excitation can be used.

Figure 12 shows the frequency response curves in terms of mean square values for $\alpha = 0°$. They are calculated using the same method in [11] when $x_g(t)$ in (4) and (7) is replaced by the harmonic excitation $a_0 \cos \omega t$. When $a_0 = \sqrt{2\pi S_0/\gamma}$, the harmonic excitation has the same amount of energy as that of the random excitation, referred to as "equivalent harmonic excitation". Figure 12 corresponds to Fig. 5, when $a_0 = 0.00458$. The solid and broken lines represent the stable and unstable steady-state solutions, respectively. Figures 12(a) and 12(b) show the mean square values of the harmonic oscillations of b_{10} and b_{01}, respectively, in the nonlinear coupled system, and Figs. 12(c) and 12(d) in the nonlinear uncoupled system. When $\alpha = 0°$, only (1, 0) mode is excited as shown in Figs. 12(c) and 12(d), and this corresponds to the nonlinear uncoupled system "▲" in Fig. 5. However, in Fig. 12(b), the steady-state solution of (0, 1) mode is unstable along branch "B_2C_2" and this mode is autoparametrically excited along stable branch "$E_2F_2C_2$". The autoparametric interaction also causes (1, 0) mode to appear at lower amplitudes along stable branch "$E_1F_1C_1$" in Fig. 12(a), and this corresponds to the nonlinear coupled system "○" in Fig. 5.

Figure 13 shows the mean square values of the harmonic oscillations of b_{10} and b_{01}, when only the value

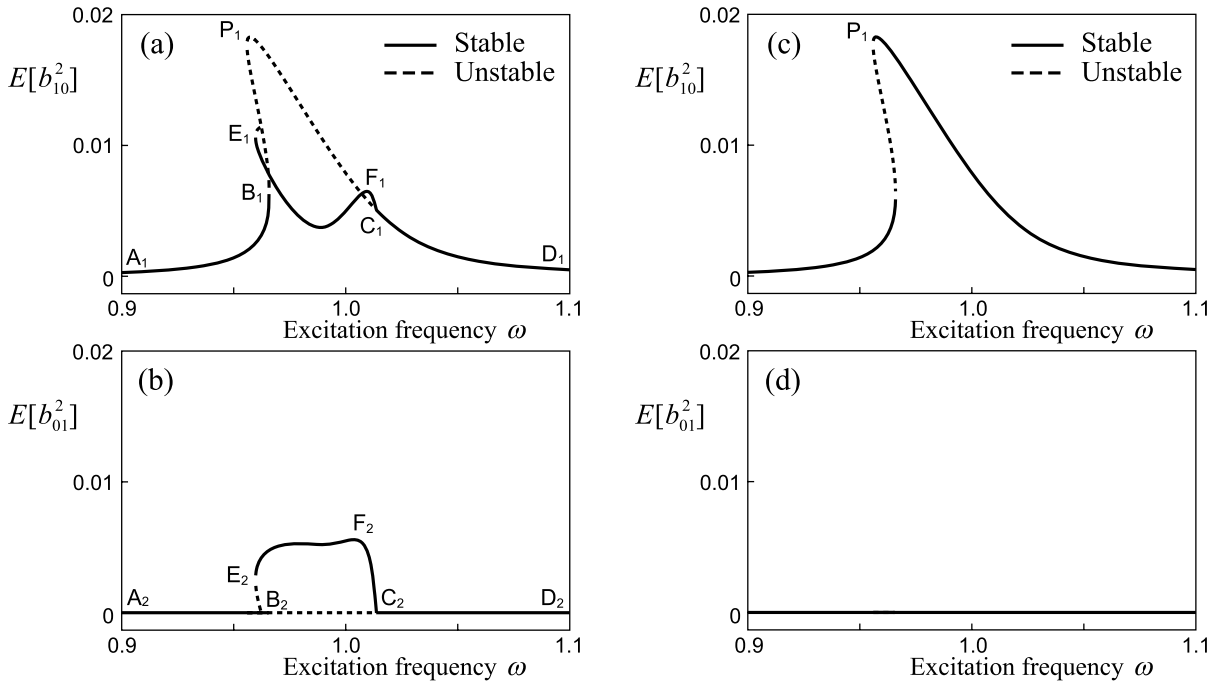

Fig. 12 Frequency response curves corresponding to Fig. 5 for $\alpha = 0°$. (**a**) $E[b_{10}^2]$ for (1, 0) mode and (**b**) $E[b_{01}^2]$ for (0, 1) mode in the nonlinear coupled system; (**c**) $E[b_{10}^2]$ for (1, 0) mode and (**d**) $E[b_{01}^2]$ for (0, 1) mode in the nonlinear uncoupled system

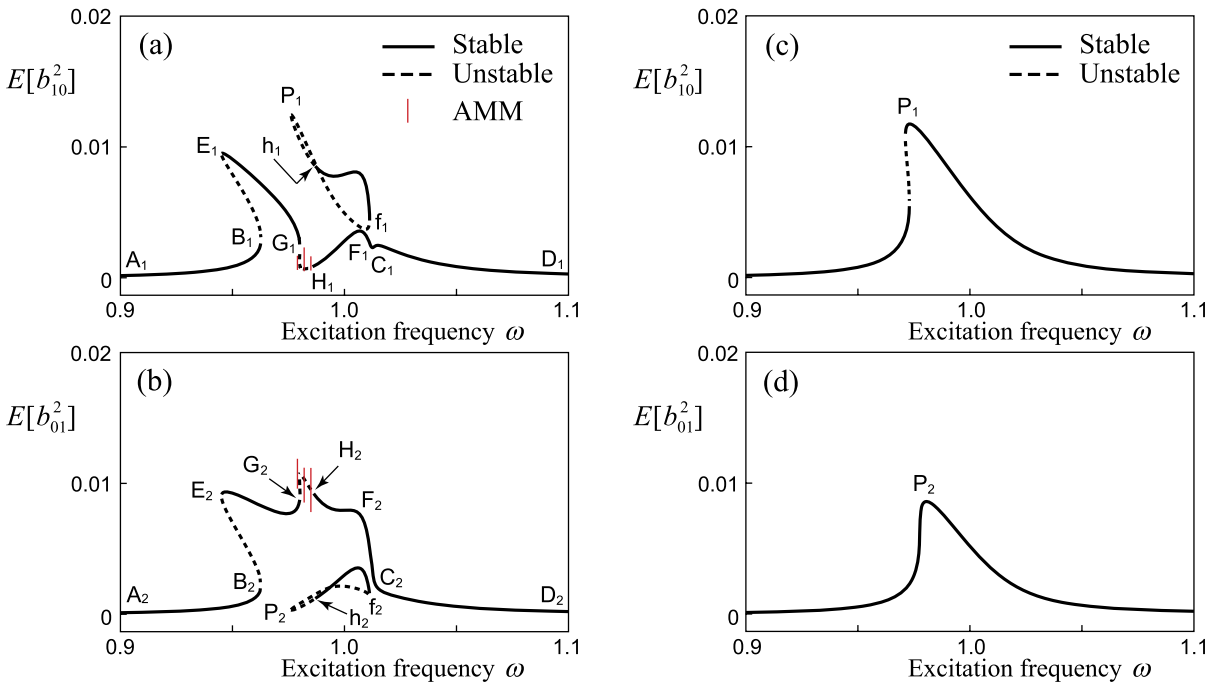

Fig. 13 Frequency response curves corresponding to Fig. 8 for $\alpha = 40°$. (**a**) $E[b_{10}^2]$ for (1, 0) mode and (**b**) $E[b_{01}^2]$ for (0, 1) mode in the nonlinear coupled system; (**c**) $E[b_{10}^2]$ for (1, 0) mode and (**d**) $E[b_{01}^2]$ for (0, 1) mode in the nonlinear uncoupled system

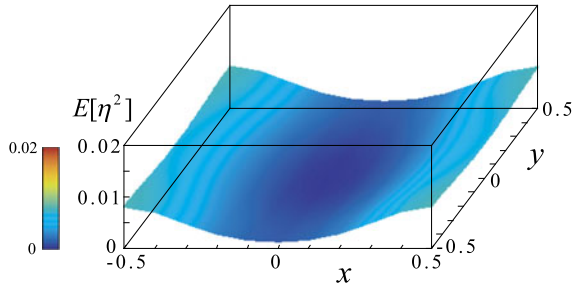

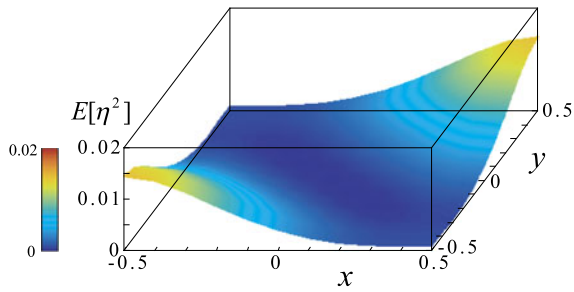

Fig. 14 3D distribution charts of $E[\eta^2]$ at $\Omega = 0.98$. (**a**) $\alpha = 0°$ in Fig. 5, (**b**) $\alpha = 40°$ in Fig. 8

of α is changed from $\alpha = 0°$ in Fig. 12 to 40° and corresponds to Fig. 8. Both modes oscillate in Figs. 13(c) and 13(d), and (1, 0) mode appears at slightly higher amplitudes than those of (0, 1) mode because it receives slightly more energy from the harmonic excitation. This result is similar to "▲" in Fig. 8. The results of Figs. 13(a) and 13(b) are more complicated, however, it is clear that as the excitation frequency ω increases, (0, 1) mode oscillates at higher amplitudes along branch "E_2C_2" than those of (1, 0) mode along "E_1C_1". This result, where (1, 0) mode receives more energy from the excitation but appears at lower values than (0, 1) mode, is similar to that of "○" in Fig. 8. The difference between the nonlinear coupled and uncoupled systems may be attributed to the autoparametric interaction and (1, 1) mode. Note that amplitude modulate motions (AMMs) appear over interval "G_iH_i" ($i = 1, 2$) with modulated amplitudes plotted by vertical thin lines. Furthermore, isolated loops "$P_ih_if_iP_i$" appear and may correspond to (1, 0) mode oscillating less frequently at higher amplitudes than (0, 1) mode as seen in Fig. 9.

Figures 14(a) and 14(b) show the three-dimensional (3D) distribution charts of the mean square values $E[\eta^2]$ for $\alpha = 0°$ and 40°, respectively, when the other values of the system parameters are the same as those in Figs. 5 and 8. $E[\eta^2]$ includes $E[\eta_x^2]$ and $E[\eta_y^2]$, which are measured at positions $(x, y) = (1/2, 0)$ and $(0, w/2)$, respectively. It can be seen that (1, 0) mode predominantly appears for $\alpha = 0°$ because sloshing appears at high amplitudes on the right and left tank walls as shown in Fig. 14(a). Both (1, 0) and (0, 1) modes predominantly appear for $\alpha = 40°$ and the liquid elevations are higher at the two opposite corners as shown in Fig. 14(b).

Figure 15 shows the probability density functions (PDFs), $p(\eta_x)$ and $p(\eta_y)$, at $\Omega = 0.98$. The curve consisting of "●" is obtained by averaging 100 PDFs each calculated from a time history. The solid curves represent the Gaussian PDFs which are calculated using the mean values and the variances of the time histories of η_x and η_y. Figure 15(a) corresponds to Fig. 5 for $\alpha = 0°$. In the upper graph of Fig. 15(a), the simulation results of $p(\eta_x)$ are asymmetric and deviate from the Gaussian PDF due to the nonlinearity of sloshing. The negative liquid elevation η_x appears during $-0.16 < \eta_x < 0$, while the positive liquid elevation η_x appears from 0 to over 0.2. Therefore, the positive liquid elevation appears at larger amplitudes than the negative elevation, as illustrated in the time history of η_x in Fig. 4. In the lower graph of Fig. 15(a), the full scale of the vertical axis is 50 to clearly show the simulation results of $p(\eta_y)$. Note that these results deviate significantly from the Gaussian PDF and appear at large values near $\eta_y = 0$ due to the autoparametric interaction. This corresponds to η_y intermittently oscillating, as shown in Fig. 4. Figure 15(b) corresponds to Fig. 8 for $\alpha = 40°$. Here, $p(\eta_x)$ slightly deviates from the Gaussian PDF near $\eta_x = 0$, while $p(\eta_y)$ is nearly identical to the Gaussian PDF. This implies that the nonlinearity of sloshing influences (1, 0) mode more significantly than (0, 1) mode. The negative and positive elevations of both $p(\eta_x)$ and $p(\eta_y)$ are symmetrical, and this result is also reflected in their time histories.

In order to evaluate the risk of liquid overspill from square tanks, Fig. 16 shows the three-dimensional distribution charts of the mean square values $E[\eta_{\max}^2]$ of the maximum liquid elevation $\eta_{\max}$ in the xy-plane at $\Omega = 0.98$. The other values of the system parameters are the same as those in Figs. 5 and 8. When $\alpha = 0°$ in Fig. 16(a), sloshing occurs at mid levels at all four corners of the tank. It is thus unlikely that liquid will overspill. When $\alpha = 40°$ in Fig. 16(b), sloshing occurs at high levels at the two opposite tank corners due

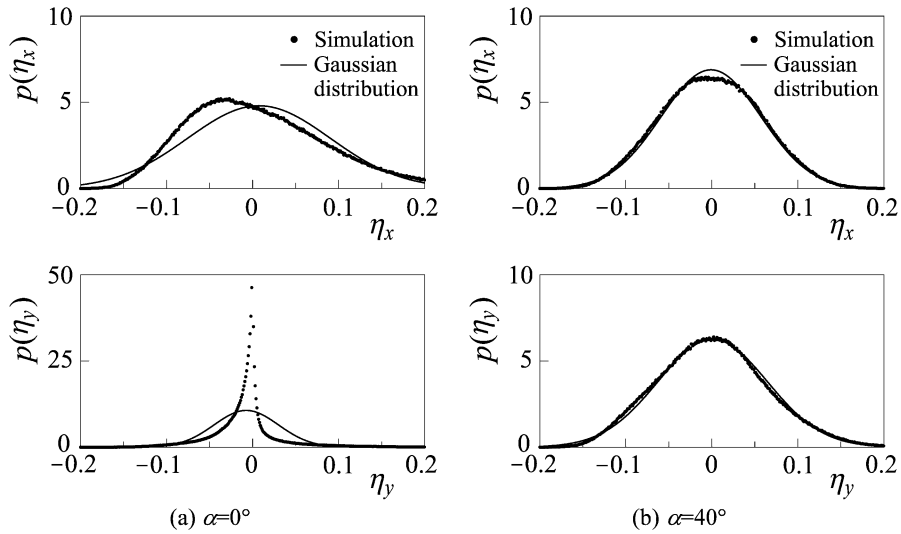

Fig. 15 Probability density distributions of the liquid elevations η_x and η_y showing the influence of the excitation direction α at $\Omega = 0.98$. (**a**) $\alpha = 0°$ in Fig. 5, (**b**) $\alpha = 40°$ in Fig. 8

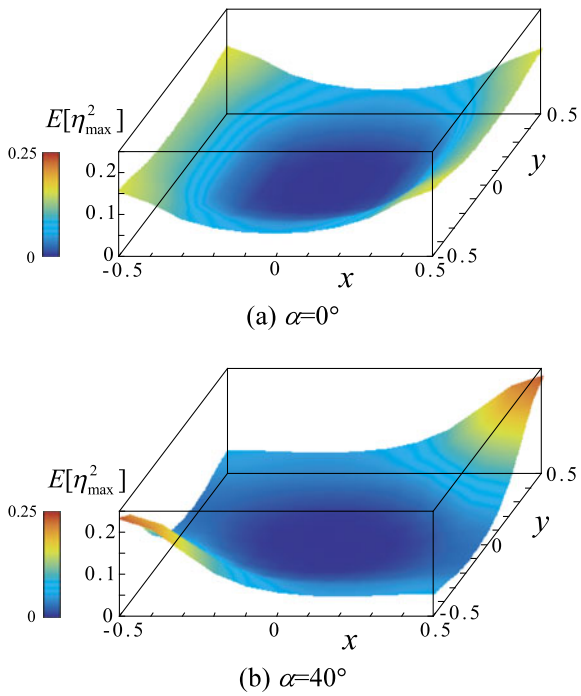

Fig. 16 3D distribution charts of $E[\eta^2_{\max}]$ at $\Omega = 0.98$. (**a**) $\alpha = 0°$ in Fig. 5; (**b**) $\alpha = 40°$ in Fig. 8

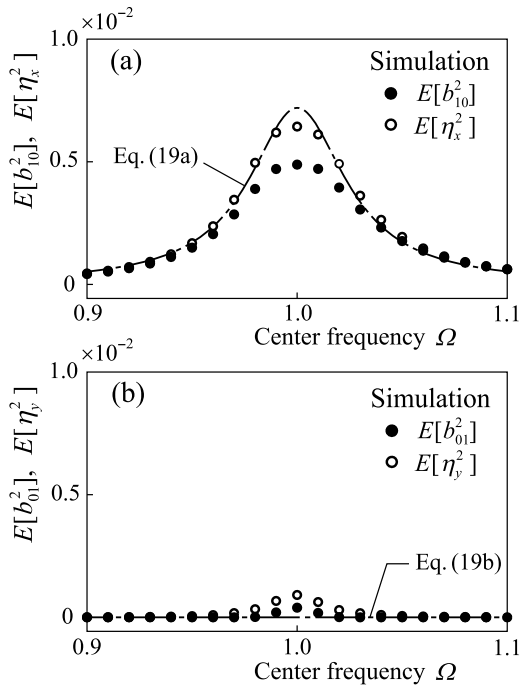

Fig. 17 Same as Fig. 5 for $\alpha = 0°$, but $h = 0.34$. (**a**) $E[b^2_{10}]$ and $E[\eta^2_x]$ for (1, 0) mode; (**b**) $E[b^2_{01}]$ and $E[\eta^2_y]$ for (0, 1) mode

to both (1, 0) and (0, 1) modes oscillating at nearly the same high amplitudes. Therefore, the risk of liquid overspill is severe compared with that of Fig. 16(a). These distribution charts can be used to predict where the liquid may spill out of the tank. Furthermore, these charts can be used to estimate where extreme pressures may act on the tank walls and ceiling in the case of hermetically sealed tanks, and can be used as guidelines for designing liquid storage tanks.

3.3 Influence of liquid level

It is well known that the liquid level plays a significant role in governing the nonlinear dynamics of slosh-

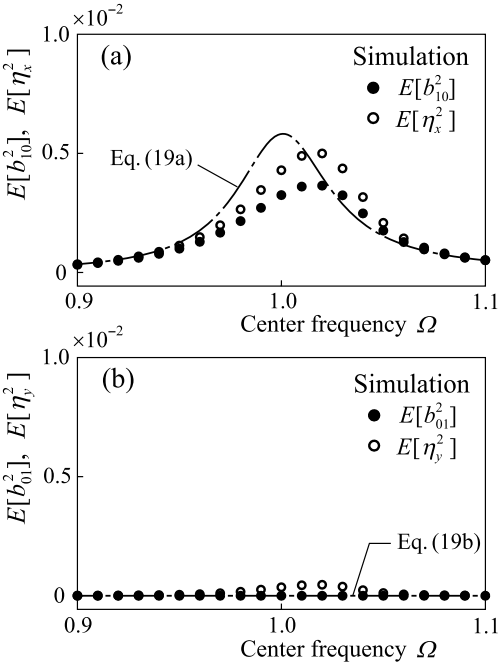

Fig. 18 Same as Fig. 5 for $\alpha = 0°$, but $h = 0.28$. (**a**) $E[b_{10}^2]$ and $E[\eta_x^2]$ for (1, 0) mode; (**b**) $E[b_{01}^2]$ and $E[\eta_y^2]$ for (0, 1) mode

ing. In order to investigate the influence of the liquid level on sloshing in square tanks subjected to random ground excitation, Figs. 17 and 18 show the mean square responses for $h = 0.34$ and 0.28, respectively. The other values of the system parameters are the same as those in Fig. 5 for $\alpha = 0°$. In Fig. 17 for a mid liquid level, the mean square values symmetrically appear on both sides of $\Omega = 1.0$ and deviate slightly from the theoretical curves (19a), (19b) near the peaks. Although the autoparametric interaction still causes (0, 1) mode to appear, it appears at lower values than those in Fig. 5. As h is decreased further, the peak of the mean square values $E[\eta_x^2]$ shifts slightly to the right for a low liquid level as shown in Fig. 18. Furthermore, the mean square values $E[b_{01}^2]$ are nearly equal to 0. Thus, as the liquid level is decreased, sloshing occurs at lower amplitudes and the autoparametric interaction is less effective. From Figs. 5, 17, and 18, it can be assumed that a critical level h_c exists at which the nonlinear system behaves like the linear system as in Fig. 17. When $h > h_c$ as in Fig. 5, "○" deviates from (19a), (19b) and behaves like a soft-spring type, whereas when $h < h_c$ as in Fig. 18, "○" deviates from (19a), (19b) and behaves as a hard-spring type. It is thus important to consider the nonlinearity of sloshing in order to achieve the most accurate results.

4 Concluding remarks

The mean square responses of the two predominant sloshing modes, (1, 0) and (0, 1) modes, in square tanks have been investigated when the tanks are subjected to horizontal, random ground excitation. The excitation is generated from the response of a second-order linear filter to a white Gaussian random noise. The results can be summarized as follows:

1. When the bandwidth of the random ground excitation is narrow and the excitation direction α is 0°, only (1, 0) mode receives energy from the ground excitation. The autoparametric interaction occurs, and it causes (0, 1) mode to appear and the mean square responses of (1, 0) mode to decrease when the center frequency of the excitation is close to the natural frequencies of these two modes.
2. Increasing the bandwidth results in less autoparametric interaction and the system responses are similar to those in the corresponding linear system. In addition, the mean square responses of both modes flatten.
3. When $0° < \alpha < 45°$, although both modes are directly excited, (1, 0) mode receives more energy from the ground excitation than (0, 1) mode. However, the mean square values of (1, 0) mode are not always larger than those of (0, 1) mode. This is due to the amount of energy exchanged between (1, 0) and (0, 1) modes through the internal resonance.
4. When the bandwidth is comparatively narrow, the system responses under random ground excitation can be confirmed by using the frequency response curves for the system under equivalent harmonic excitation.
5. When $\alpha = 0°$, (0, 1) mode intermittently oscillates and its PDF significantly deviates from the Gaussian distribution because of the autoparametric interaction. However, when α increases, the PDFs of both modes approach the Gaussian distributions and they behave like those of a linear system.
6. Distribution charts of the mean square responses of the liquid elevation are shown. They can predict where liquid overspill and high hydrodynamic pressure may occur in square tanks.

7. Comparatively high and low liquid levels cause the peak of the system to appear slightly to the left or right of the center frequency, respectively. A critical liquid level likely exists at which the system behaves similar to a corresponding linear system.

For further work, the influences of the intensity of the random ground excitation and the aspect ratio of the tank cross-section should be investigated as well as the risk of liquid overspill most likely to occur at two opposing corners of the tank. Furthermore, real seismic excitation can be applied to this model in order to investigate the responses to earthquakes.

References

1. Ibrahim, R.A., Pilipchuk, V.N., Ikeda, T.: Recent advances in liquid sloshing dynamics. Appl. Mech. Rev. **54**, 133–199 (2001)
2. Housner, G.W.: Dynamic pressures on accelerated fluid containers. Bull. Seism. Soc. Am. **47**(1), 15–35 (1957)
3. Tedesco, J.W., Landis, D.W., Kostem, C.N.: Seismic analysis of cylindrical liquid storage tanks. Comput. Struct. **32**(5), 1165–1174 (1989)
4. Haroun, M.A.: Vibration studies and tests of liquid storage tanks. Earthq. Eng. Struct. Dyn. **11**(2), 179–206 (1983)
5. Hutton, R.E.: An investigation of resonant, nonlinear, nonplanar free surface oscillations of a fluid. NASA Technical Note D-1870, 1–64 (1963)
6. Abramson, H.N.: The dynamic behavior of liquids in moving containers. NASA SP-106 (1966)
7. Faltinsen, O.M.: A non-linear theory of sloshing in rectangular tanks. J. Ship Res. **18**(4), 224–241 (1974)
8. Hayama, S., Aruga, K., Watanabe, T.: Nonlinear response of sloshing in rectangular tanks (1st report, Nonlinear response of surface elevation). Bull. JSME **26**(219), 1641–1648 (1983)
9. Faltinsen, O.M., Rognebakke, O.F., Timokha, A.N.: Resonant three-dimensional nonlinear sloshing in a square-base basin. J. Fluid Mech. **487**, 1–42 (2003)
10. Faltinsen, O.M., Rognebakke, O.F., Timokha, A.N.: Classification of three-dimensional nonlinear sloshing in a square-base tank with finite depth. J. Fluids Struct. **20**(1), 81–103 (2005)
11. Ikeda, T., Ibrahim, R.A., Harata, Y., Kuriyama, T.: Nonlinear liquid sloshing in a square tank subjected to obliquely horizontal excitation. J. Fluid Mech. **700**, 304–328 (2012)
12. Ibrahim, R.A.: Liquid Sloshing Dynamics. Cambridge University Press, Cambridge (2005)
13. Dalzell, J.F.: Exploratory studies of liquid behaviour in randomly excited tanks—Lateral excitation. NASA-CR-88534, TR-2, pp. 1–51 (1967)
14. Sakata, M., Kimura, K., Utsumi, M.: Non-stationary response of non-linear liquid motion in a cylindrical tank subjected to random base excitation. J. Sound Vib. **94**(3), 351–363 (1984)
15. Sakata, M., Kimura, K., Utsumi, M.: Non-stationary random responses of an elastic circular cylindrical liquid storage container to a simulated earthquake excitation. In: Proceedings 11th International Conference on Structural Mechanics and Reactor Technology, K, K35/6, Tokyo, Japan, pp. 571–576 (1991)
16. Kimura, K., Utsumi, M., Sakata, M.: Nonstationary responses of nonlinear liquid motion in a circular cylindrical tank to stochastic earthquake excitation with two-directional components. In: Proceedings International Conference on Nonlinear Stochastic Dynamics, Hanoi, Vietnam, pp. 159–168 (1995)
17. Utsumi, M., Kimura, K., Sakata, M.: Stochastic response analysis of an elastic rectangular container with an internal liquid to simulated seismic excitation. J. Sound Vib. **96**(1), 83–99 (1984)
18. Utsumi, M., Kimura, K., Sakata, M.: The nonstationary random vibration of an elastic circular cylindrical liquid storage tank in simulated earthquake excitation (straightforward analysis of tank wall deformation). JSME Int. J., Ser. III **30**(261), 467–475 (1987)
19. Chen, W., Haroun, M.A., Liu, F.: Large amplitude liquid sloshing in seismically excited tanks. Earthq. Eng. Struct. Dyn. **25**(7), 653–669 (1996)
20. Wang, C.Z., Khoo, B.C.: Finite element analysis of two-dimensional nonlinear sloshing problems in random excitations. Ocean Eng. **32**(2), 107–133 (2005)
21. Sriram, V., Sannasiraj, S.A., Sundar, V.: Numerical simulation of 2D sloshing waves due to horizontal and vertical random excitations. Appl. Ocean Res. **28**, 19–32 (2006)
22. Nasar, T., Sannasiraj, S.A., Sundar, V.: Liquid sloshing dynamics in barge carrying container subjected to random wave excitation. J. Nav. Archit. Mar. Eng. **9**(1), 43–65 (2012)
23. Soundararajan, A., Ibrahim, R.A.: Parametric and autoparametric vibrations of an elevated water tower: Part III, Random response. J. Sound Vib. **121**(3), 445–462 (1988)
24. Ibrahim, R.A., Soundararajan, A.: Non-linear parametric liquid sloshing under wide band random excitation. J. Sound Vib. **91**(1), 119–134 (1983)
25. Ikeda, T., Ibrahim, R.A.: Nonlinear random responses of a structure parametrically coupled with liquid sloshing in a cylindrical tank. J. Sound Vib. **284**(1–2), 75–102 (2005)
26. Ikeda, T., Harata, Y., Ibrahim, R.A.: Nonlinear responses of sloshing in square tanks subjected to horizontal random ground excitation. In: Proceedings of International Conference on Structural Nonlinear Dynamics and Diagnosis, Marrakech, Morocco, April 30–May 2 (2012)
27. Crandall, S.H., Mark, W.D.: Random Vibration in Mechanical Systems. Academic Press, New York (1963)
28. Box, G.E.P., Muller, M.E.: A note on the generation of random normal deviates. Ann. Math. Stat. **29**(2), 610–611 (1958)